Appl. Phys. A (2016) 122:325
DOI 10.1007/s00339-016-9821-4

Applied Physics A
Materials Science & Processing

# Effect of the KOH chemical treatment on the optical and photocatalytic properties of $BiVO_4$ thin films

R. Mirabal-Rojas[1,2] · O. Depablos-Rivera[1,2] · S. M. Thalluri[3] · J. C. Medina[1,2] · M. Bizarro[1] · J. Perez-Alvarez[1] · S. E. Rodil[1] · A. Zeinert[4]

Received: 25 September 2015 / Accepted: 30 October 2015 / Published online: 9 March 2016


**Abstract** In this work, we present the structural, optical and photocatalytic properties of $BiVO_4$ thin films produced by a dual-magnetron sputtering process using both $Bi_2O_3$ (α-phase, 99.98 % purity) and V (99.9 % purity) targets under $Ar/O_2$ atmosphere with a ratio of 18:2. The films were deposited varying the power applied to the targets to obtain stoichiometric films, and the monoclinic structure was achieved by post-deposition annealing. The dual process was chosen to better control the Bi/V ratio since Bi and V have very different sputtering yields. In particular, the influence of a chemical treatment using potassium hydroxide (KOH) on the optical properties and different dye discolorations (acid blue 113 and methyl orange) is discussed. The optical properties were studied by reflectance and transmittance spectroscopy, where the spectra were fitted to obtain the refractive index dispersion and the optical band gap of the $BiVO_4$ as a function of the film structure, as determined by X-ray diffraction and Raman spectroscopy.

✉ R. Mirabal-Rojas
mirabalroberto@yahoo.com

[1] Instituto de Investigaciones en Materiales, Universidad Nacional Autónoma de México, Mexico City, Mexico

[2] Posgrado en Ciencia e Ingeniería de Materiales, Universidad Nacional Autónoma de México, Mexico City, Mexico

[3] Department of Applied Science and Technology (DISAT), Politecnico di Torino, Torino, Italy

[4] Laboratoire de Physique de la Matière Condensée, Université de Picardie Jules Verne, Amiens, France

## 1 Introduction

In recent years, bismuth vanadate, $BiVO_4$ has received a lot of interest because the material has shown significant visible-light-driven photocatalytic activity [1–5], but more important because it has been predicted that the monoclinic-$BiVO_4$ (mc-$BiVO_4$) phase could function as an ideal semiconductor to drive solar water splitting process, with the subsequent production of hydrogen [6–9]. However, experimentally, it has been found that the photoelectrochemical current densities of unmodified $BiVO_4$ photoanodes tested in electrolytes without hole acceptors ranged only between 0.1 and 1.8 $mA/cm^2$ (AM 1.5G, 1 sun 1.23 V vs RHE), too far away from values of technological interest [7, 10]. The low photocurrents have been associated to high electron–hole recombination, poor charge transport properties and/or inadequate water oxidation kinetics [7]. Conventionally, $BiVO_4$ has been obtained by solid-state reaction [10], obtaining $BiVO_4$ nanostructures with a wide variety of morphologies and sizes, which are later deposited to form photoanodes. One possible explanation of the low photocurrents is that the film quality attained by these methods is not ideal for the application. Thus, more recently, thin film deposition methods such as pulsed laser deposition [11, 12] and magnetron sputtering [13–16] have also been applied. Particularly, the deposition by dual-magnetron sputtering seems to be a promising method [13]. Thalluri et al. [16] found photocurrents of unmodified mc-$BiVO_4$ of 1.1 $mA/cm^2$, just by processing the sputtered films using a three-step process: deposition at low substrate temperature, 2 h annealing at 400 °C, and a chemical KOH treatment. A brief explanation about the effect of the chemical treatment was presented in that paper [16], but definitely not all the details are completely understood yet. In the present work, further analysis considering the effect

of the KOH treatment on both the optical properties and topographical features of the mc-$BiVO_4$ is given. Moreover, considering that the KOH treatment has a strong effect on the visible-light-driven water splitting, we did also investigate its effect on the photocatalytic properties for degrading dye solutions.

## 2 Experimental details

The films were prepared by dual-magnetron sputtering, using two targets (2″): α-$Bi_2O_3$ and vanadium, with purity of 99.9 and 99.5 %, respectively. The deposition was done under $Ar/O_2$ reactive atmosphere using a gas flow ratio of 18:2; the total working pressure was 0.7 Pa. Each target had an independent power supply; this allows setting the composition of the films. Common glass was used as the substrates, except for the photoelectrochemical measurements where FTO substrates were used. The preheating substrates temperatures explored were: RT, 100, 200 and 300 °C. The power applied to the oxide target was either 30 or 50 W using radio frequency (RF), and the V target power was varied between 100 and 300 W. The films of each condition set were post-annealed at 400 °C for 2 h in air. After exploration of the different deposition conditions, the most adequate conditions to obtain the mc-$BiVO_4$ phase were: 160 and 30 W for V and $Bi_2O_3$, respectively, without preheating of the substrates. After the annealing, to obtain the monoclinic phase, the films were immersed in 1 M KOH solution for 40 min, and then, they were rinsed with distilled water for a few minutes and finally were dried using $N_2$ gas. The structure, roughness and optical properties of the mc-$BiVO_4$ films were measured before and after the KOH treatment. The X-ray diffraction (XRD) patterns were obtained using a Rigaku Ultima IV diffractometer at grazing incident angle (1°) with a Cu $K_\alpha$ radiation ($\lambda = 1.5418$ Å). The Micro-Raman characterization was performed using an En-Spectra R532 spectrometer at excitation wavelength of 532 nm. The surface topography was measured by atomic force microscopy (AFM) using a Jeol JSPM-5200 microscope. The cantilevers used were V-shaped silicon model NSC15 with a vertex angle of 20° and a radius of curvature of 10 nm with a shape of a square pyramidal. Scanning areas of $10 \times 10$ and $5 \times 5$ $\mu m^2$ were measured. Moreover, the roughness was measured using a Dektak 150 mechanical profilometer at a scanning length of 250 μm.

Transmittance ($T$) and reflectance ($R$) spectra were collected with two spectrophotometers. Specular transmittance ($T_s$) and reflectance ($R_s$) spectra were recorded using a Jasco V670 in a configuration that allows measurements to be taken in the same spot of the sample. Moreover, the total transmittance $T_t$ including the contribution of the diffusive transmission was measured by placing the film at the entrance of the integrating sphere. On the other hand, diffusive and total reflectance spectra were obtained using a Cary 5E (Varian) instrument. The spectra were fitted using commercial software. The $R$ and $T$ spectra of the glass substrate were separately fitted to increase accuracy of the film data fits.

As the films exhibited strong light scattering, two different model approaches were tested. In the first one, the total reflectance and transmittance were analyzed while in the second one, only the specular spectra of $R_s$ and $T_s$ were considered adding to the model an amplitude loss function to take into account the scattering. In both models, a homogenous bulk layer and a porous surface layer were assumed. The porous layer was described by an effective medium approximation using a Bruggeman model [17] mixing the dielectric function of the bulk layer and air. The bulk layer was described with a Tauc–Lorentz model [18, 19] and Kim oscillators [20], and the dielectric function was checked for Kramers–Kronig consistence.

The photocatalytic activity of the mc-$BiVO_4$ films was evaluated before and after the KOH treatment. The activity was evaluated by measuring the percentage of discoloration of the dye solution by following the absorbance spectra of the solution every 30 min. Two common organic dyes were used: methyl orange, MO ($C_{14}H_{14}N_3NaO_3S$), and acid blue 113, AB ($C_{32}H_{21}N_5Na_2O_6S_2$), both from Sigma-Aldrich. The dye solution concentration was fixed at $1 \times 10^{-5}$ M for the MO and $0.5 \times 10^{-5}$ M for the AB, while two pHs were evaluated: 3.5 and 7.5. The films were placed in pairs back-to-back inside a vial with 10 mL of the dye solution and exposed to a UV light lamp (26 $Wm^{-2}$).

## 3 Results

Table 1 presents a short summary of the results obtained when the different powers and substrate temperatures were used during the deposition. Briefly, the films were amorphous when the substrates were not preheated and crystalline in the opposite case. For a fixed power of 50 W applied to the $Bi_2O_3$ target, it was found that at low powers applied to the V target (<150 W), the films were basically bismuth oxide ($Bi_2O_3$) films, while at higher power (>200 W), the samples showed segregated metallic bismuth and vanadium oxide. Using 175 W on the V target, the mc-$BiVO_4$ was found after annealing the films at 400 °C for 2 h in air, but in coexistence with residual signals from bismuth oxide, indicating an excess of bismuth. Therefore, the power applied to the bismuth oxide target was decreased from 50 to 30 W, which indeed reduced the presence of the $Bi_2O_3$ phase. Nevertheless, the obtained mc-$BiVO_4$ phase contained residual signal from

**Table 1** Summary of the deposition conditions, the post-annealing and the identification from XRD and Raman spectroscopy data

| V target DC power (*W*) | $Bi_2O_3$ target RF power (*W*) | Grown at RT | Grown at 100–300 °C | Grown at RT post-annealed (2 h) |
|---|---|---|---|---|
| 100 | 50 | Amorphous | Mainly $Bi_2O_3$ | |
| 150 | 50 | Amorphous | Predominantly $Bi_2O_3$ | |
| 200, 300 | 50 | Amorphous | Bi + $VO_x$ | |
| 175 | 50 | Amorphous | | 100–200 °C: amorphous<br>300 °C unstable<br>400 °C: mc-$BiVO_4$ + $Bi_2O_3$ excess |
| 175 | 30 | Amorphous | | mc-$BiVO_4$ + excess of V |
| 155–165 | 30 | Amorphous | | mc-$BiVO_4$ + $VO_x$ |

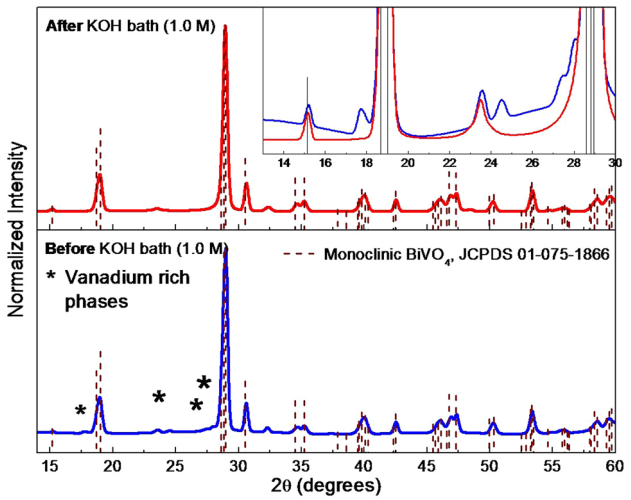


**Fig. 1** X-ray diffraction patterns of the sputtered $BiVO_4$ thin films before (Bf) and after (Af) the KOH treatment. The monoclinic pattern is the predominant phase in both cases. The inset shows an amplification of the region where ill-defined $VO_x$ signals can be observed

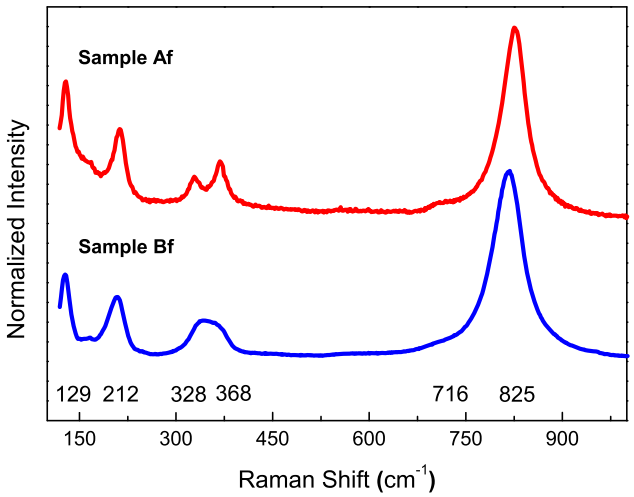


**Fig. 2** Raman spectra for the mc-$BiVO_4$ thin films before (Bf) and after (Af) the KOH treatment. The spectra were obtained using a 532-nm laser for samples deposited on glass

vanadium oxide. Efforts to tune more precisely the composition, varying the deposition power of the V target between 155 and 165 W, while keeping the $Bi_2O_3$ target fixed at 30 W, did not improve the quality of the films. Therefore, it was decided to use the KOH chemical etching process as a method to preferentially remove the $VO_x$ excess phase to the samples deposited at 160 W (V)–30 W ($Bi_2O_3$). After adjustment of both the concentration and the etching time, the diffraction patterns for the mc-$BiVO_4$ films obtained before (Bf) and after (Af) the KOH treatment are shown in Fig. 1. The monoclinic $BiVO_4$ phase is clearly identified in both patterns (JCPDS 01-075-1866); however, for sample Bf, there are other peaks which correspond to vanadium rich phases, more clearly observed in the inset of Fig. 1. Similarly, the Raman spectra before and after the KOH treatment are shown in the Fig. 2. The spectrum from sample Bf confirms the presence of the monoclinic phase, but the signals at 328 and 368 $cm^{-1}$, corresponding to the symmetric and antisymmetric bending modes of $VO_4^{3-}$ [21, 22], are not well defined. After the chemical treatment, all the peaks from the mc-$BiVO_4$ phase are clearly defined and slightly thinner. These results are in good agreement with those previously reported for the $BiVO_4$ samples deposited at 165 W (V)–30 W ($Bi_2O_3$) to which a similar process was applied obtaining an enhancement in the photocurrent [16]. It is important to mention that the enhancement in the photocurrent was also confirmed for the samples studied in this paper.

As stated in the Introduction, in this paper, the interest was placed on the evaluation of the changes induced in the photocatalytic, optical and topographical properties of the mc-$BiVO_4$ films before and after the KOH treatment.

The AFM images are shown in the Fig. 3 (10 × 10 μm), where it can be seen that after the KOH treatment, the average roughness of the films was reduced nearly to half the original value. Such results were consistent with

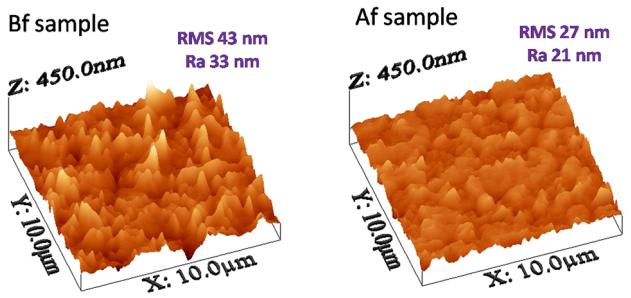


**Fig. 3** Atomic force microscopy images of the mc-$BiVO_4$ thin films before (Bf) and after (Af) the KOH treatment. The roughness values: average (Ra) and root-mean-square (RMS) are indicated next to each figure

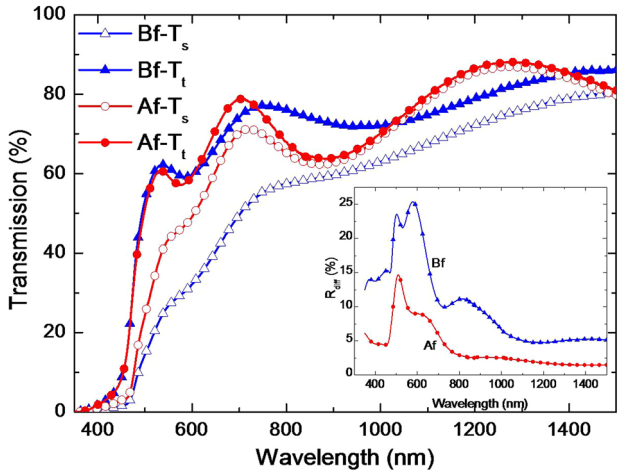


**Fig. 4** Optical transmittance spectra for both samples (Bf and Af) as a function of the wavelength. The specular ($T_s$) and total ($T_t$) spectra are presented to show that after the KOH treatment, the surface layer was strongly modified. The *inset* shows the $R_{diff}$ spectra, where $R_{diff}$ is the difference between the total reflectance, $R_t$ and the specular reflectance $R_s$

measurements taken at lower scale (5 × 5 µm) showing a reduction in the root-mean-square roughness (RMS) from 52 to 26 nm. Similarly, larger 2D scans (250 µm) were performed using the profilometer to find a reduction in the RMS value from 25 ± 9 to 9 ± 1 nm.

Figure 4 presents the transmission spectra of the two films (Bf and Af). In both cases, specular transmission $T_s$ is lower than the total transmission $T_t$, and this difference decreases with wavelength. When subtracting $T_s$ from $T_t$, a curve can be obtained which approximately follows the $1/\lambda^4$ law of Rayleigh scattering. However, the effect is significantly stronger before the KOH treatment than after. This difference in the scattering behavior is confirmed by the reflectance data shown in the inset of Fig. 4. It shows the pure diffusive reflectance (skipping the specular component of reflection) of both films. Diffusive reflectance is much higher for the Bf sample than for the Af film. For the

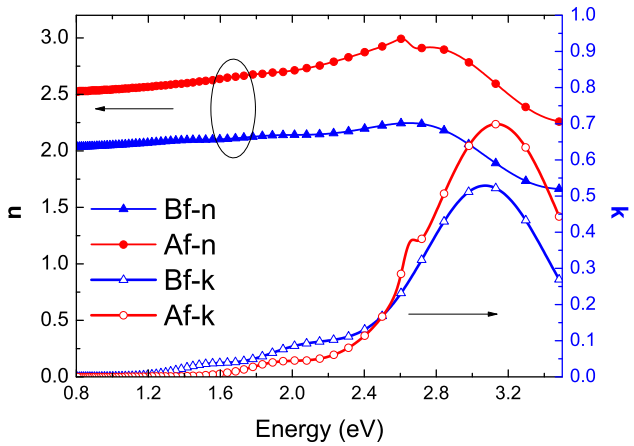


**Fig. 5** Refractive index, $n$ and extinction coefficient, $k$ for the mc-$BiVO_4$ thin films before (Bf) and after (Af) the KOH treatment

first, the reflectance has virtually no specular component above 500 nm (<3 %).

Strong scattering behavior in thin films can lead to misinterpretations of optical data when not carefully analyzed. Therefore, we modeled the data in two independent ways: as explained above, either the total $R_t$ and $T_t$ response were analyzed, or only the respective specular components for $R_s$ and $T_s$ were considered. $R_s$ and $T_s$ were fitted by adding a scattering surface model via a simple loss function of the amplitude,

$$\frac{C_1}{1+\frac{X}{C_2}} \tag{1}$$

where $C_1$ and $C_2$ are free parameters and X is the wavenumber ($cm^{-1}$). Both models provided very similar data of the dielectric function with minor differences (<5 %) for the refractive index $n$ and the extinction coefficient $k$. Figure 5 exhibits $n$ and $k$ for both films as a function of the energy (eV) in the investigated spectral range. At 800 nm, one observes refractive indexes around 2.1 and 2.6 for the Bf and Af samples, respectively. Absorption ($k$) starts at lower energies for the Bf sample and is significantly higher than for the Af film below the gap. Following the relationship between the absorption coefficient $\alpha$ and $k$

$$\alpha = 4\pi k/\lambda \tag{2}$$

one finds values of $\alpha$ above 6000 $cm^{-1}$ at 1.25 eV for the Bf sample which is already a rather strong absorption level for sub-gap energies.

The band edge $E_g$ was estimated through the relationship for direct allowed transitions

$$(\alpha h\nu)^2 = (h\nu - E_g) \tag{3}$$

In Fig. 6, a direct band gap can be identified for the Bf film around 2.65 eV while two gaps are visible for the Af

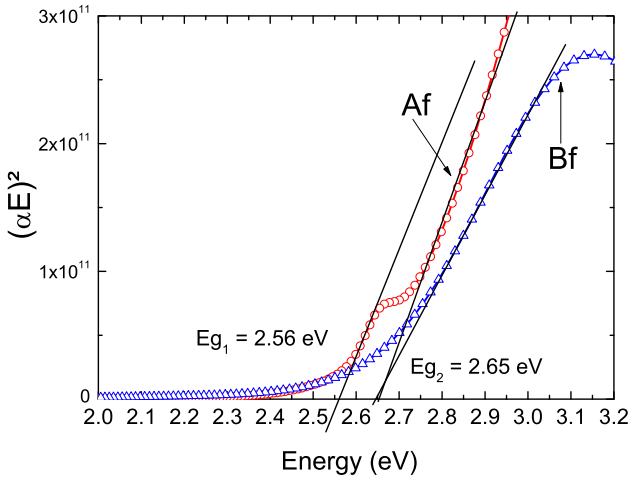


**Fig. 6** Estimation of the direct optical band gap for the mc-$BiVO_4$ thin films before (Bf) and after (Af) the KOH treatment

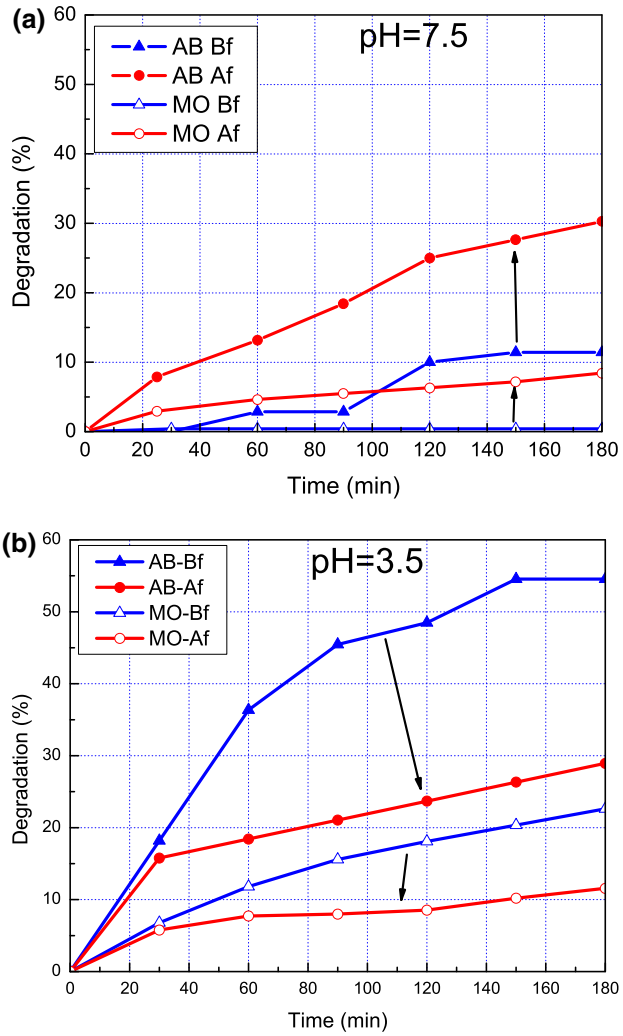


**Fig. 7** Percentage of dye discoloration as a function of the immersion time. The experiment was done illuminating the samples with UV light and for two different pHs; **a** pH = 7.5 and **b** pH = 3.5. The dye concentrations were for acid blue 113, AB ($0.5 \times 10^{-5}$ M), and for the methyl orange, MO ($1 \times 10^{-5}$ M). The results for the samples before (Bf) and after (Af) the KOH treatment are shown for both pHs

sample, the 2.65 eV gap but also a lower one around 2.56 eV.

The optical data also gave some insight into the topography of the films. First, the fits confirmed the change of film thickness with KOH treatment; the Bf film exhibits a total thickness of 406 nm compared to 270 nm for the Af film. These values are consistent with those measured by profilometry. Moreover, in both films, a porous surface layer was necessary to obtain best fits. For the Bf sample, this layer was 87 nm thick with a void volume of 48 %. Meanwhile, for the KOH-treated sample, the porous layer thickness was 76 nm (void volume 26 %). Finally, the loss function, which parameterized the scattering effect for the specular $R_s$ and $T_s$ spectra reveals a stronger scattering for the Bf film (Bf: $C_1 = 1.018$, $C_2 = 81{,}399\ \text{cm}^{-1}$, Af: $C_1 = 1.031$, $C_2 = 160{,}527\ \text{cm}^{-1}$).

Figure 7 shows the percentage of degradation of the dyes as a function of the immersion time. The photocatalytic activity of the mc-$BiVO_4$ films at nearly neutral pH was almost negligible, less than 30 % (Fig. 7a), but for both dyes a slight increment was observed after the KOH treatment. On the other hand, for the acidic pH (pH = 3.5), a better photocatalytic performance of the mc-$BiVO_4$ films was obtained for both dyes. The maximum degradation obtained was about 50 % for the AB after 180 min using the mc-$BiVO_4$ films before the KOH treatment. Contrary to the results at pH = 7.5, the degradation was reduced after the KOH treatment for both dyes.

## 4 Discussion

While a lot of diffusive reflectance spectra of $BiVO_4$ powders have been published [23–27], reliable optical data of $BiVO_4$ thin films are scarce [14, 15, 28, 29]. Theoretical studies mostly focus on the electronic properties of monoclinic $BiVO_4$ [30–33] as this phase seems to be the most promising for photocatalytic applications. A direct band gap is predicted with values varying between 2.15 eV [30, 32] and 2.48 eV [33]. The later value has been confirmed by diffusive reflectance spectroscopy (Kubelka–Munk analysis) for powders while X-ray spectroscopy provided 2.38 eV [34]. Cooper et al. [33] found a theoretical gap about 2.5 eV and compared it to the experimental value of 2.48 eV derived from X-ray absorption spectroscopy (XAS) and X-ray emission spectroscopy on thin films grown by chemical vapor deposition [33]. Zhao et al. [31] calculated the dielectric function for different polarizations and found a strong anisotropy with gap values between 2.5 and 3 eV and about 2.6 eV for polycrystalline material.

From diffuse reflectance spectra of mc-$BiVO_4$ powder samples, band gaps are reported around 2.4–2.5 eV [23, 24, 26, 34] while for zircon-like tetragonal phase is about 2.9 eV [23, 25, 27]. For polymorph samples with mixed phases, the gap can vary from 2.4 to 2.9 eV [25, 27].

The value $E_g$ of 2.65 eV found for the Bf film is slightly higher than what is observed for pure mc-$BiVO_4$ powders. Luo et al. [28] found 2.54 eV for mc-$BiVO_4$ thin films prepared by a polymer-assisted chemical solution approach, but Singh et al. [15] measured 2.68 eV in RF sputtered films exhibiting XRD and Raman characteristics of mc-$BiVO_4$. A hypothetical contribution of a weak tetragonal phase which could explain the higher band gap value is unlikely in view of our XRD patterns. However, the Raman spectra clearly show that some of the peaks are ill defined for the Bf sample (the asymmetric and symmetric deformation modes of $VO_4^{3-}$ tetrahedron are not well resolved). Furthermore, the red shift of the stretching V–O mode (around 825 $cm^{-1}$) suggests a longer V–O bond length. It is now well established that the band gap is governed by the Bi 6s, O 2p and V 3d atomic orbitals [30, 32, 33]. Thus, a slight increase in $E_g$ could be caused by a smaller delocalization of the electron and hole pairs and a smaller overlapping between the Bi 6s and O 2p orbitals, as observed by Thalluri et al. [26] and Hernandez et al. [29].

When KOH treatment is applied, the Raman and XRD peaks show a better-defined mc-$BiVO_4$ and the gap shifts toward a lower value of 2.56 eV which is closer to the reported literature value (although there is still a 2.65 eV component detectable). The refractive index of 2.6 (at 800 nm) is also in a better agreement with the literature data for mc-$BiVO_4$ [31, 35] in contrast to the value of 2.1 for the sample before the KOH treatment. Finally, the sub-band region also provides a hint about the microstructure. Admittedly, mc-$BiVO_4$ is known for exhibiting a soft rise of $\alpha$ below the gap, resulting from a range of weak valence to conduction band transitions [30], so the much higher absorption observed for the Bf sample can be linked to the poor crystal quality compared to the KOH-treated film.

The photocatalytic activity of mc-$BiVO_4$ has been extensively reported for nanostructures and less for thin films. Moreover, comparison of results is difficult since the conditions used are specific of each experiment. In general, good (above 60 %) visible-light photodegradation of a variety of organic molecules has been demonstrated, being the organic dyes the most commonly used contaminants. One feature that has been studied is the dependence of the photocatalytic activity on the morphology (shape and size) and obviously the associated surface area [2]. It has been shown that the morphology of the nanoparticles changes the crystallographic facets that are preferentially exposed on the surface and, for example, NPs that exhibited more facets of the {010} planes have been found to improve the adsorption and degradation of the organic molecules [36, 37]. Such results have been explained in terms of the atomic density of such facets and/or the dangling bonds at the surface [31], as well as to the relative fraction of acidic/basic sites on the surface [38]. These results remind us that the photocatalytic process proceeds at the surface of the photocatalyst; therefore, even for the same basic material, different activities can be obtained depending on the surface properties [37, 39].

In this work, we have shown that the photocatalytic activity of the mc-$BiVO_4$ thin films is not as good as their nanostructured counterparts. The maximum degradation obtained was 50 % in 180 min for the AB ($0.5 \times 10^{-5}$ M) in acidic solutions using the Bf sample. The lower degradation in comparison with the reported mc-$BiVO_4$ nanostructures could be associated with the lower surface area of the thin films. However, it is important to mention that in our group, higher percentages have been achieved using $Bi_2O_3$ thin films evaluated under the same experimental conditions [40]. Our expectations were that the photocatalytic activity could be improved after the KOH treatment since the measured photocurrents suggested lower electron–hole recombination and/or better transport charge properties. However, the results were disappointing. For the pH = 3.5, the photodegradation activity was reduced after the KOH treatment for both dyes, which could be ascribed as a secondary effect of the reduced surface area. Profilometry and AFM showed that a major consequence of the KOH treatment was the modification in the surface topography, lower roughness which is in agreement with the larger porosity detected by optical measurements of the Bf sample (48 %) in comparison with the Af sample (26 %). These two data suggested a lower surface area and therefore a reduced surface for the adsorption of the dye molecules. Nevertheless, other factors, such as the fraction of acidic/basic sites or the preferential surface planes could have been also modified by the KOH treatment. The thickness was strongly reduced, and the chemical etching process could also occur through preferential crystallographic planes. Moreover, the role played by the acidic sites was confirmed by the measured different response for the two pHs. At more acidic pH, the dye molecules can be easily adsorbed on the surface due to the protonation of the acidic sites, explaining the larger degradation, this is a well-known phenomenon. The interesting result here is that the photocatalytic activity after the KOH treatment was slightly increased at pH = 7.5, while at pH = 3.5, it was reduced. Such a different behavior is an indication that the KOH treatment did also modify the surface charges of the films. As a confirmation, a titration experiment [41] was performed to evaluate the point of zero charge (pzc; the pH at which the surface charge is neutral) of the mc-$BiVO_4$ films before and after the KOH treatment, finding that there

was a slight reduction from 8.4 (Bf sample) to 7.2 (Af sample). Above the pzc, the surface charge is positive and vice versa, it is negatively charged below the pzc, i.e., more acidic sites [42].

Summarizing, the photocatalytic properties are often balanced between crystallinity quality, available surface area and the surface electronic structure of the topmost surface layer. While the first is crucial for uphill reactions such as water oxidation, the latter becomes more important for downhill reactions such as pollutant degradation. This competition between bulk-surface properties may explain why the KOH treatment of our mc-$BiVO_4$ films leads to significant reduction in the photocatalytic activity, while promoting the photoelectrochemical current density.

## 5 Conclusions

The KOH treatment implemented to improve the photocurrent obtained from the sputtered mc-$BiVO_4$ photoanodes induced variations in both the optical and surface properties.

From the optical properties, we can conclude that the KOH treatment can be considered as a chemical etching process that reduces the film thickness, but also increases the crystal quality of the monoclinic $BiVO_4$ phase.

The analysis of the surface topography indicated that the surface roughness was reduced to about half of its initial value, decreasing therefore the specific surface area of the films.

The photocatalytic properties of the sputtered mc-$BiVO_4$ are lower than other oxide thin films, and the KOH treatment could not be used to significantly enhance the photocatalytic degradation of organic pollutants. One possible explanation for the lower degradation at acidic pH is the reduced specific area which leads to less adsorption of the molecules. However, the slight increment observed at neutral pH coupled with the reduction in the pzc after the KOH treatment indicates that other surface properties were also modified.

**Acknowledgements** The research leading to these results has received funding from the European Community Seven Framework Programme (FP7-NMP-2010-EU-MEXICO) and CONACYT under Grand Agreements Nos. 263878 and 125141 (BisNano), respectively. Economical support for this work was also provided by the PHOCSCLEEN project 318977. The authors acknowledged technical support from A. Tejeda, H. Zarco, C. Flores and A. Fonseca.

## References

1. U.M. García-Pérez, S. Sepúlveda-Guzmán, A. Martínez-de la Cruz, Solid State Sci. **14**, 293–298 (2012)
2. X. Lin, L. Yu, L. Yan, H. Li, Y. Yan, C. Liu, H. Zhai, Solid State Sci. **32**, 61–66 (2014)
3. Z.J. Zhang, W.Z. Wang, M. Shang, W.Z. Yin, Catal. Commun. **11**, 982–986 (2010)
4. W.Z. Wang, S. Meng, M. Tan, L.J. Jia, Y.X. Zhou, S. Wu, X.W. Huang, Y.J. Liang, H.L. Shi, Appl. Phys. A **118**, 1347–1355 (2015)
5. J.Z. Yin, S.B. Huang, Z.C. Jian, M.L. Pan, Y.Q. Zhang, Z.B. Fei, X.R. Xu, Appl. Phys. A **120**, 1529–1535 (2015)
6. S.J.A. Moniz, S.A. Shevlin, D.J. Martin, Z.-X. Guo, J. Tang, Energy Environ. Sci. **8**, 731–759 (2015)
7. T.S. Sinclair, B.M. Hunter, J.R. Winkler, H.B. Gray, A.M. Muller, Mater. Horiz. **2**, 330–337 (2015)
8. R. van de Krol, M. Graetzel, *Photoelectrochemical Hydrogen Production*, 1st edn. (Springer, Dordrecht, 2012), pp. 205–212
9. Z.-F. Huang, L. Pan, J.-J. Zou, X. Zhang, L. Wang, Nanoscale **6**, 14044–14063 (2014)
10. Y. Park, K.J. McDonald, K.-S. Choi, Chem. Soc. Rev. **42**, 2321–2337 (2013)
11. A.J.E. Rettie, S. Mozaffari, M.D. McDaniel, K.N. Pearson, J.G. Ekerdt, J.T. Markert, C.B. Mullins, J. Phys. Chem. C **118**, 26543–26550 (2014)
12. D.B. Chrisey, G.K. Hubler, *Pulsed Laser Deposition of Thin Films*, 1st edn. (Wiley, New York, 1994)
13. L. Chen, E. Alarcón-Lladó, M. Hettick, I.D. Sharp, Y. Lin, A. Javey, J.W. Ager, J. Phys. Chem. C **117**, 21635–21642 (2013)
14. S. Sarkar, N.S. Das, K.K. Chattopadhyay, Solid State Sci. **33**, 58–66 (2014)
15. A.P. Singh, N. Kodan, A. Dey, S. Krishnamurthy, B.R. Mehta, Int. J. Hydrogen Energy **40**, 4311–4319 (2015)
16. S.M. Thalluri, R.M. Rojas, O.D. Rivera, S. Hernández, N. Russo, S.E. Rodil, Phys. Chem. Chem. Phys. **17**, 17821–17827 (2015)
17. D.A.G. Bruggeman, Ann. Phys. **24**, 636–664 (1935)
18. G.E. Jellison, F.A. Modine, Appl. Phys. Lett. **69**, 371–373 (1996)
19. H. Chen, W.Z. Shen, Eur. Phys. J. B **43**, 503–507 (2005)
20. C.C. Kim, J.W. Garland, H. Abad, P.M. Raccah, Phys. Rev. B **45**, 11749–11767 (1992)
21. F.D. Hardcastle, I.E. Wachs, H. Eckert, D.A. Jefferson, J. Solid State Chem. **90**, 194–210 (1991)
22. A. Zhang, J. Zhang, Mater. Sci. Pol. **27**, 1015–1023 (2009)
23. A. Kudo, K. Omori, H. Kato, J. Am. Chem. Soc. **121**, 11459–11467 (1999)
24. S. Tokunaga, H. Kato, A. Kudo, Chem. Mater. **13**, 4624–4628 (2001)
25. J.Q. Yu, Y. Zhang, A. Kudo, J. Solid State Chem. **182**, 223–228 (2009)
26. S.M. Thalluri, C.M. Suarez, M. Hussain, S. Hernandez, A. Virga, G. Saracco, N. Russo, Ind. Eng. Chem. Res. **52**, 17414–17418 (2013)
27. Z.Q. Wang, W.J. Luo, S.C. Yan, J.Y. Feng, Z.Y. Zhao, Y.S. Zhu, Z.S. Li, Z.G. Zou, CrystEngComm **13**, 2500–2504 (2011)
28. H.M. Luo, A.H. Mueller, T.M. McCleskey, A.K. Burrell, E. Bauer, Q.X. Jia, J. Phys. Chem. C **112**, 6099–6102 (2008)
29. S. Hernández, S.M. Thalluri, A. Sacco, S. Bensaid, G. Saracco, N. Russo, Appl. Catal. A Gen. **504**, 266–271 (2015)
30. A. Walsh, Y. Yan, M.N. Huda, M.M. Al-Jassim, S.H. Wei, Chem. Mater. **21**, 547–551 (2009)
31. Z.Y. Zhao, Z.S. Li, Z.G. Zou, Phys. Chem. Chem. Phys. **13**, 4746–4753 (2011)
32. K.N. Ding, B. Chen, Y.L. Li, Y.F. Zhang, Z.F. Chen, J. Mater. Chem. A **2**, 8294–8303 (2014)
33. J.K. Cooper, S. Gul, F.M. Toma, L. Chen, P.A. Glans, J.H. Guo, J.W. Ager, J. Yano, I.D. Sharp, Chem. Mater. **26**, 5365–5373 (2014)
34. D.J. Payne, M.D.M. Robinson, R.G. Egdell, A. Walsh, J. McNulty, K.E. Smith, L.F.J. Piper, Appl. Phys. Lett. **98**, 212110 (2011)

35. J.F. Li, A.S. Bhalla, L.E. Gross, Opt. Commun. **92**, 115–118 (1992)
36. L. Zhang, D.R. Chen, X.L. Jiao, J. Phys. Chem. B **110**, 2668 (2006)
37. T. Liu, X. Zhou, M. Dupuis, C. Li, Phys. Chem. Chem. Phys. **17**, 23503–23510 (2015)
38. T. Saison, N. Chemin, C. Chanéac, O. Durupthy, V. Ruaux, L. Mariey, F. Maugé, P. Beaunier, J.-P. Jolivet, J. Phys. Chem. C **115**, 5657–5666 (2011)
39. L. Jing, W. Zhou, G. Tian, H. Fu, Chem. Soc. Rev. **42**, 9509–9549 (2013)
40. J.C. Medina, M. Bizarro, C.L. Gomez, O. Depablos-Rivera, R. Mirabal-Rojas, B.M. Monroy, A. Fonseca-Garcia, J. Perez-Alvarez, S.E. Rodil, Catalysis Today (2015). doi:10.1016/j.cattod.2015.10.025
41. K. Bourikas, C. Kordulis, A. Lycourghiotis, Environ. Sci. Technol. **39**, 4100–4108 (2005)
42. G.A. Parks, P.L. de Bruyn, J. Phys. Chem. **66**, 967–973 (1962)